Journal of Computing and Electronic Information Management
ISSN: 2413-1660 | Vol. 12, No. 3, 2024

Microwave Resonant Sensor Based on MCSRR Research

Dani Gao [1], Han Sun [1], Heping Huang [1,2]

[1] School of Electronic Information, Southwest University for Nationalities, Key Laboratory of Electronic Information Engineering of the State People's Committee, Chengdu 610225, Sichuan, China
[2] School of Electronic Information, Sichuan University, Chengdu 610065, Sichuan, China

Abstract: This paper presents a low-cost and easy-to-fabricate microwave resonant sensor for characterising the dielectric properties of solids and powders. The designed sensor is based on a FR-4 dielectric substrate with a Multiple Complementary Split-Ring Resonator (MCSRR) etched on its bottom, and this resonant unit is used to place the sample to be tested (Material Under Test, MUT). The sensor was operated at a resonant frequency of 4.9GHz and used the offset resonance to detect the dielectric properties of different solids and powders. The relationships established by the simulation were experimentally verified by the fabricated sensor. The percentage error between the calculated dielectric constant and the reference dielectric constant is less than 8.7% for a certain thickness of the sample to be tested, which verifies the feasibility of the proposed loaded MCSRR sensor. Therefore, this sensor is expected to be a cost-effective and convenient solution for accurate characterisation of solid, powder dielectric properties.

Keywords: Commas. microwave sensors; Multiple Complementary Split-Ring Resonator (MCSRR); Dielectric constant.

1. Introduction

With the deepening development of the modern communication field, the wide application of RF microwave technology with miniaturisation and integration characteristics of the sensor demand is becoming more and more prominent, and new materials, new processes and advanced manufacturing skills continue to emerge for the RF microwave measurement of the performance enhancement and cost reduction to provide support for the design of higher sensitivity and smaller size of the microwave resonance sensors become one of the research hotspots for scholars at home and abroad.

As a microwave passive device, the filter is an important unit for processing analogue baseband signals and has a significant impact on system performance. Among them, the band-stop filter[1-3] has the ability to attenuate signals in specific frequency bands, and also meets the performance requirements of adjustable blocking position and blocking bandwidth, which provides a core point for microwave resonant sensors. As a result of continuous exploration and research, the concept of metamaterials[4] has been developed, which is based on the design of artificial structures and the alteration of key physical dimensional parameters of materials to obtain unique functionalities. Metamaterials refer to a class of man-made materials that are incomparable to natural materials, and their origin can be traced back to Left-Handed Material (LHM)[5] . Left-handed materials refer to artificial dielectric materials with negative values of dielectric constant and magnetic permeability, and the research of D.R. Smith et al. has pushed the study of left-handed materials from theory to reality[6-10] .

Microwave resonant sensors are widely used in industrial, biological as well as electronic applications due to their good sensing properties. As researchers invest in left-handed materials, a sensor loaded with a novel left-handed material structure, Complementary Split-Ring Resonator (CSRR), is presented. Nowadays, the design of high-performance microwave resonant sensors using the unique electromagnetic properties of the CSRR structure has become a popular research direction nowadays. In order to meet the needs of applications, microwave resonant sensors not only need to have high sensitivity detection capability, but also need to achieve miniaturised design. The emergence of CSRR structure provides a new idea for the design of microwave resonant sensors with higher sensitivity and smaller size.

Through the joint efforts of researchers at home and abroad, the topics based on CSRR structure become more and more perfect and mature. At present, CSRR-based sensors are widely used in such fields as biosensing[11-15] , pressure detection[16] , displacement detection[17-21] , temperature detection[22] , dielectric detection[23-27] and gas-sensitive detection[28-30] . According to the above background, the main content of this paper is the research and design of microwave resonant sensors based on the loaded MCSRR structure. Compared with the current grating or optical fibre[31-33] sensors, the microwave sensors based on the MCSRR structure have the features of smaller physical dimensions, easy integration, higher measurement accuracy, and relatively simple data processing. The above features significantly reduce the measurement cost of microwave resonant sensors, and the requirements for the measurement environment are significantly reduced. In addition, these features simplify the entire measurement process by reducing the tedious preliminary preparation work[34-40] .

Based on this, this paper proposes a dielectric constant measurement sensor based on a Multiple Complementary Split-Ring Resonator (MCSRR) structure, and gives the frequency response of the sensor by analysing its equivalent circuit model. Based on theoretical calculations as well as electromagnetic field simulations, it is demonstrated that the coupling capacitance between the resonators can enhance the sensitivity of the sensor in detecting the change of dielectric constant. Therefore, the sensor is machined and fabricated and tested, and the simulation and test results achieve good agreement. This part of the work verifies the feasibility of the proposed loaded MCSRR sensor. The design principle of the sensor, system analysis in sensing and experimental validation of the proposed sensor are presented in Sections II, III and IV, respectively.

2. Sensor design principles

A. Structural design and simulation analysis of the sensor

As shown in Fig. 1, the microwave resonant sensor structure proposed in this chapter consists of a defective copper foil ground plane on one side of the substrate (bottom), while a microstrip line is formed on the other side of the substrate (top), where Port 1 and Port 2 are used for inputs and outputs at both ends, respectively. The dielectric plate material is FR-4 with a relative permittivity of 4.4 and dimensions of 22mm*15mm*0.5mm; the MCSRR resonator unit consists of two mutually symmetrical CSRRs with "T" shaped grooves to enhance the coupling, which are jointly etched on the ground plane of the Cu foil (thickness of the Cu foil is 35 um). The microstrip line consists of a merge circuit and two branch circuits, where the width of the merge circuit is t and the width of the branch circuit is w; the characteristic impedance of the merge circuit is designed to be $50\,\Omega$ for the purpose of port matching. In order to eliminate the signal reflection at the connection between the combined and branch microstrip lines, the characteristic impedance of the branch microstrip line is designed as $100\,\Omega$.

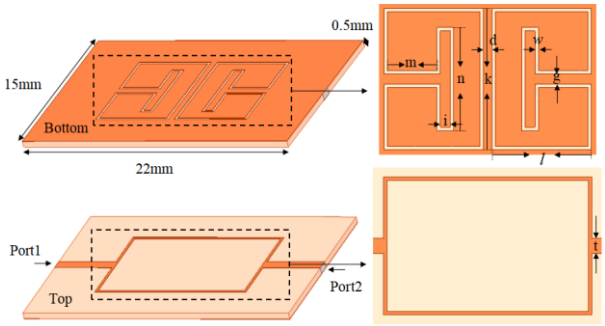

Fig. 1 Schematic diagram of MCSRR based sensor

The physical dimensions shown in Fig. 1 are: $k = 8.5\text{mm}$, $l = 6\text{mm}$, $d = 0.5mm$, $w = 0.2mm$, $g = 0.6\text{mm}$, $m = 3\text{mm}$, $n = 6.2\text{mm}$, $i = 0.6\text{mm}$, $t = 0.92mm$. The sample to be tested is placed on the resonator unit, which is in direct contact with the resonator during the actual simulation and measurement.

The resonant frequency of the sensor is affected by three parameters of the resonant ring m, n and i, which mainly affect the capacitance and conductivity of the sensor and together control the resonant frequency. Therefore, the HFSS software is used to scan the above parameters respectively, so that its frequency is controlled at around 4.9GHz under no load, and the results of its S21 parameters at no load are shown in Fig. 2.

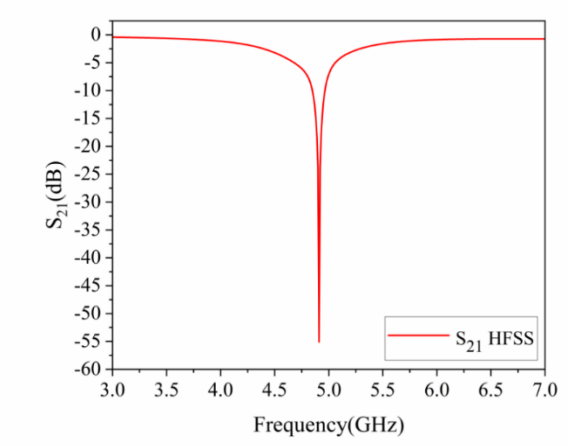

Fig. 2 Scanning results based on MCSRR sensor S21

To investigate the underlying physical principles, the field distributions are plotted in Fig. 3.

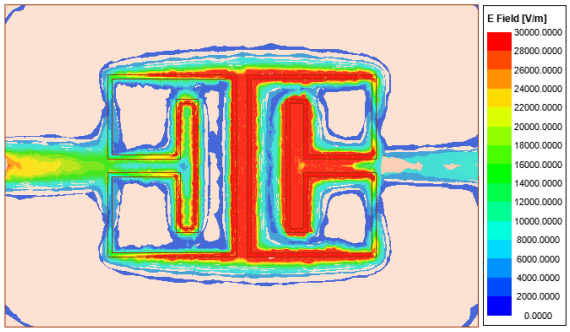

Fig. 3 Electric field distribution at 4.9GHz based on MCSRR sensor

It can be clearly seen that more energy is coupled to the resonant unit, i.e. the electromagnetic field is concentrated at the location of the measuring MUT, which enhances the interaction between the field and the sample to be measured.

Next, the relationship between dielectric constant and resonant frequency was observed by loading samples to be tested with different dielectric constants. Here, the MUT covers the entire resonant unit to prevent any electric field from leaking into the air to degrade the sensitivity of the sensor. Its dielectric constant is set from 1 to 10 in intervals of 1 and the loss angle tangent is kept as 0. The simulation results are shown in Fig. 4.

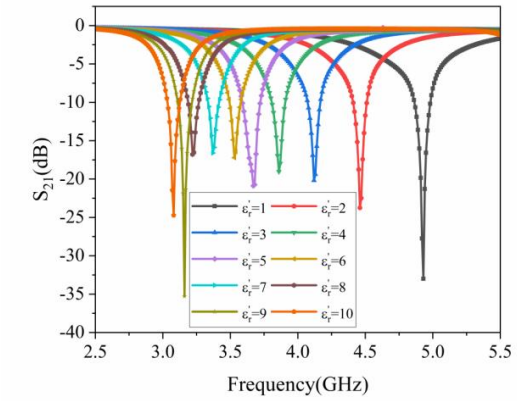

Fig. 4 Dielectric constant in the range 1-10 for S21

Observation of the above figure clearly shows that as the dielectric constant gradually increases, the resonant frequency shows a corresponding decreasing trend. This is not difficult to explain because the increase in dielectric

constant causes the equivalent capacitance of the whole structure to increase, thus decreasing the resonant frequency.

B. Equivalent circuit simulation verification of the sensor

The structure of a microwave sensor can be thought of as a parallel combination of inductance and capacitance. Thus, it acts as a band reject filter at resonance, i.e., it exhibits maximum attenuation. The equivalent circuit model is used to calculate the required dimensions of the microwave sensor to resonate at the desired frequency. By analysing this, the equivalent circuit of the sensor can be obtained and the equivalent circuit is shown in Fig. 5.

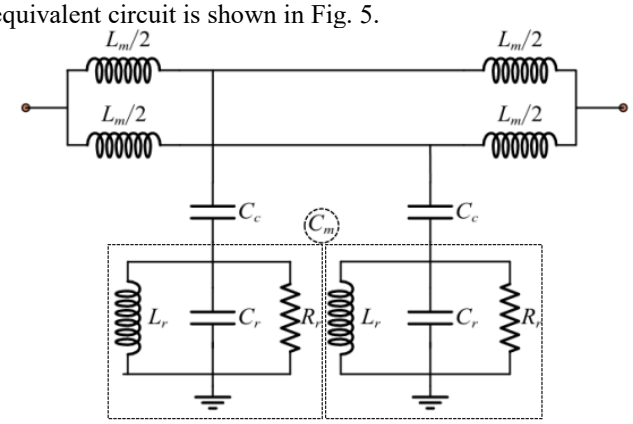

Fig. 5 Equivalent circuit diagram of open and closed circuit microstrip line loaded MCSRR, where $L_r = 0.915\text{nH}$, $C_r = 0.89\text{pF}$, $L_m = 2.74\text{nH}$, $C_c = 0.22\text{pF}$, $C_m = 0.099\,\text{pF}$

In the figure, L_r , C_r and R_r represent the equivalent inductance, capacitance and resistance of the CSRR, L_m represents the inductance of the open-close microstrip line, C_c represents the coupling capacitance between the open-close microstrip line and the CSRR, and C_m represents the coupling capacitance between two CSRRs. Due to the addition of the coupling capacitance C_m , the resonant frequency of the sensor is changed as shown in Eq. (1):

$$f_r = \frac{f_{r0}}{\sqrt{1 - C_m/(C_r + C_c)}} \qquad (1)$$

By extracting the values of each component in the equivalent circuit model, the correctness of the equivalent circuit simulation and resonant frequency calculation formula can be verified. Firstly, the electromagnetic field simulation of the sensor model based on the MCSRR open-close circuit microstrip line is carried out using the HFSS software; secondly, the relevant component values are preliminarily extracted based on the equivalent circuit parameter extraction method introduced in the literature; finally, the optimisation function in the ADS software is used to compare the S21 parameters of the equivalent circuit simulation and the electromagnetic field simulation until the optimal situation is fitted. The results are shown in Fig. 6.

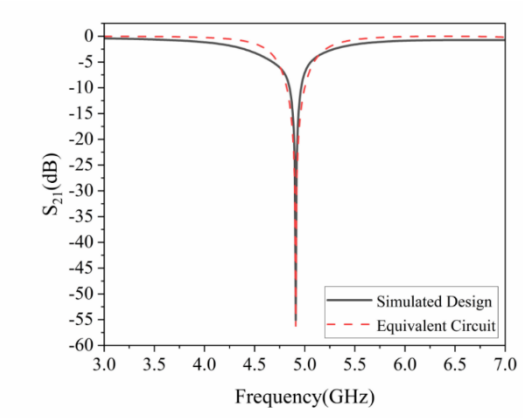

Fig. 6 MCSRR sensor simulation based design with equivalent circuit of S21

As can be seen from the figure, the equivalent circuit element values calculated according to the microwave circuit theory and optimised by the ADS software, the S21 parameters are better than the band resistance designed by the HFSS software simulation. This is because in the process of simulation design, the setting of air box boundary conditions may affect the solution area, resulting in the deviation of the calculation amount and time required for simulation, as well as the correctness of simulation. Overall, Fig. 6 demonstrates the consistency of the EMF simulation and equivalent circuit simulation trends, and the correctness of the equivalent circuit simulation and resonant frequency calculation formulas is verified.

3. Sensor system analysis

A. Quality factor analysis of sensors

As we have learnt from the previous analyses, the resonance unit of the sensor is the region where the maximum electric field is stored. In order to measure the dielectric properties of a material, the sample to be measured should be placed in the high electric field region of the sensor. As the electric field is perturbed by the sample to be measured, the capacitance of the sensor will increase due to the placement of the dielectric material, and the increase in capacitance will depend on the complex dielectric constant of the sample to be measured itself, which will result in a decrease in the resonance frequency, as shown in Eq. (1). Thus, the presence of any dielectric material can be detected by the shift in resonant frequency caused by the change in capacitance, while the loss characteristics of the dielectric material are quantified by the change in Q-factor response.

In fact, the dielectric constant consists of two parts as shown in Eq. (2):

$$\varepsilon_r = \varepsilon_r^{'} - j\varepsilon_r^{''} = \varepsilon_r^{'}(1 - j\tan\delta) \qquad (2)$$

Where $\varepsilon_r^{'}$ is the real part, known as the dielectric constant, $\varepsilon_r^{''}$ is the imaginary part, also known as the loss factor, and $\tan\delta$ is the loss angle tangent, i.e., $\tan\delta = \varepsilon_r^{''}/\varepsilon_r^{'}$. The quality factor at resonance Q_{MUT} depends on the loss angle tangent $\tan\delta$. The quality factor Q_{MUT} is related to the no-load quality factor Q_U involving S21 as in Eq. (3):

$$Q_{MUT} = Q_U\left[1 - 10^{\frac{S_{21}}{20}}\right] \qquad (3)$$

Where $Q_U = f_r / \Delta f_{3dB}$, f_r is the resonance frequency and Δf_{3dB} is the bandwidth at -3dB.

B. Sensitivity of the sensor Analyses

The most intuitive performance indicator for measuring a sensor's dielectric constant is sensitivity, which is defined as the ratio of the change in resonant frequency to the change in dielectric constant of the sample to be measured. The formula for sensitivity (S) is:

$$S = \frac{\Delta f_r}{\Delta \varepsilon_r} \tag{4}$$

In terms of mathematical modelling, this can be specifically defined as Eq. (5):

$$S_{av,f} = \frac{f_{Empty} - f_{MUT}}{f_{Empty}\left(\varepsilon_r^{'} - 1\right)} \times 100\% \tag{5}$$

The above equation is the normalised sensitivity expression, and f_{empty} and f_{sample} denote the resonance frequencies for the case of no load and loaded MUT of the sample to be measured, respectively.

From the above, it can be seen that when the resonator unit is loaded with the sample to be measured, its equivalent capacitance value will be changed. Then, the resonance frequency f_r in Eq. (1) is derived from the resonator capacitance C_r to show the sensitivity of the resonance frequency to the change of the resonator capacitance, which reflects the sensitivity of the transducer from the side, as shown in Eq. (6) :

$$\frac{df_r}{dC_r} = \frac{f_{r0}}{2\left(C_r + C_c\right)\left[1 - C_{\mathrm{m}} / \left(C_r + C_c\right)\right]} \tag{6}$$

From the above equation, the increase of coupling capacitance C_c makes the resonant frequency of the sensor more sensitive to the change of resonator capacitance C_r, which means that the microwave sensor based on the MCSRR resonator can provide higher sensitivity.

The results of the above analysis are obtained through theoretical calculations and are verified by the following simulation using HFSS software. Combining the information of the dielectric plate and the physical dimensions of the resonator and microstrip line shown in the previous section, the sensor model is established using HFSS software. Among them, the port excitation is in the form of Wave Port, whose size is related to the width of the microstrip line, the thickness of the dielectric plate and the copper foil; the boundary conditions of the defective copper foil ground plane (bottom) and the microstrip line (top) are set to Perfect E; the air box is used for field truncation of the space, and its boundary condition is set to Radiation, and its size is set to be larger than a quarter of the wavelength at least. HFSS software only calculates the inner region of the air box, and the boundary conditions can reduce the amount of computation and the time needed for simulation, in order to improve the accuracy and efficiency of the simulation.

Next, a piece of sample to be tested with a certain dielectric constant is set on the HFSS Design model, and its dielectric constant is set to 1-12 with a spacing of 1; the permeability and loss tangent angle are set to 0; the thickness of the sample to be tested is set to 5 mm after the analysis in the previous section to ensure that the thickness will not affect the simulation results, and the area of the sample to be tested needs to cover the entire resonance region.

The above is the setting of each parameter of the sensor model, and then the parametric scanning of the dielectric constant of the sample to be measured. Through the scanning, the resonance frequency can be obtained as a function of the dielectric constant, and then the corresponding data can be calculated by using Eq. (5), and then imported into Origin software for fitting, and the fitting curve is shown in Fig. 7.

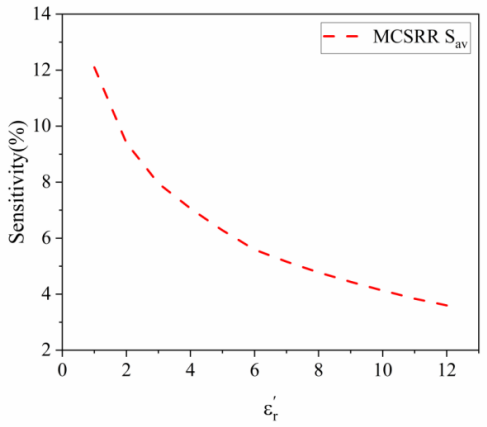

Fig. 7 Fitted curve based on the normalised sensitivity of the MCSRR sensor

The sensitivity analysis of the MCSRR-based microwave resonant sensor has been illustrated by theory and simulation, and the fabrication and experimental measurements of the physical object are carried out in the next section.

C. Extraction of sensor dielectric constant

According to the resonator theory, it is known that the offset of the resonant frequency is related to the dielectric constant of the MUT of the loaded sample to be measured. Therefore, the relationship between the resonant frequency of the sensor and the dielectric constant of the MUT can be derived analytically using its equivalent circuit model. The resonant frequency of the sensor based on the MCSRR open-circuit microstrip line is represented by Eq. (1), which shows that the sensor uses the change in the equivalent capacitance between the 2 mutually symmetric CSRRs C_m to calculate the change in the MUT dielectric constant. From Eq. (1), it can be seen that an increase in the equivalent capacitance of the MCSRR structure decreases the resonant frequency of the sensor, and a change in the dielectric constant of the MUT also causes a change in C_m. Once the structure of the sensor is determined, a relationship exists between its resonant frequency f and the dielectric constant of the sample to be measured $\varepsilon_r^{'}$ as shown in Eq. (7):

$$\varepsilon_r^{'} \propto f^{-2} \tag{7}$$

From the above equation, it can be seen that there is a linear relationship between the negative quadratic of the resonant frequency f^{-2} and the dielectric constant of the sample to be measured $\varepsilon_r^{'}$, which can be extracted.

On the HFSS Design model, the thickness of the MUT of the samples to be tested is set to 0.5, 1, 3, 5 and 10 mm, and the dielectric constants are all varied from 1 to 10 at intervals of 1 for several rounds of simulations. Next, the data for H_MUT=0.5, 1, 3, 5 and 10m are fitted linearly, and the fitted curves are shown in Fig. 8, and the linear relationship is

shown in Eq. (8):

$$f_r^{-2} = 0.03832 + 0.00764\,\varepsilon_r' \quad (8)$$

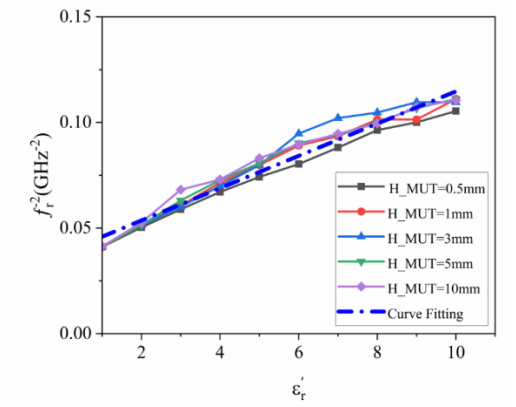

Fig. 8 Dielectric constant versus resonant frequency for different thicknesses of MUT f_r

The goodness of fit is 0.99, indicating a very good correlation between the dielectric constant and the resonant frequency in this band. Therefore, this sensor can be used for the measurement of dielectric constant in this area. In the next work, a thickness of 5 mm was selected for simulation and measurement.

4. Sensor fabrication test

After the above analyses, the MCSRR-based sensors with open and closed circuit microstrip lines exhibit good dielectric properties. Based on the physical dimensions in Section II, the physical sensor has been fabricated on FR-4 dielectric substrate by processes such as photolithography of copper foil as well as etching of Multiple Complementary Split-Ring Resonator (MCSRR) as shown in Fig. 9, and the resonance region that needs to be loaded with the samples to be tested has been labelled in Fig. 9 (a). The experimental measurements were carried out on a 3656B VNA with a frequency range of 3-7GHz.Two cables were connected to the VNA and calibrated using a 20202A 3.5mm negative head calibration piece. After calibration, the transducer was fixed to the SMA connector (Model: SMA-KHD103L) and the S21 was measured at no load , and the band-resistive resonance point at 4.9GHz is evident from Fig. 9 (c).

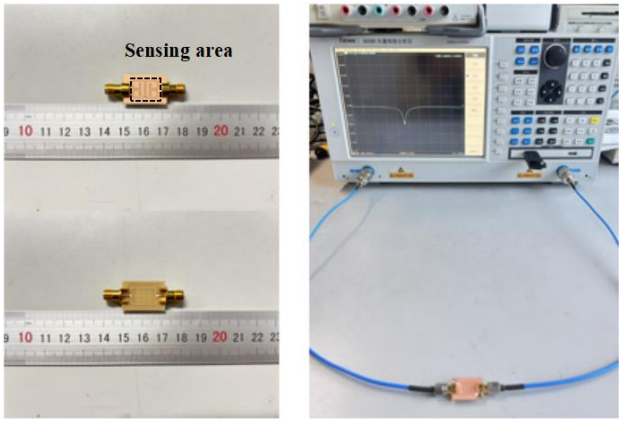

Fig. 9 Physical view of the MCSRR-based sensor (a) bottom; (b) top; (c) S21 measured by VNA at no load

With this, experimental measurements were carried out for the unloaded case and the samples to be measured. For the measurements, the samples to be measured were loaded on the resonance region of the sensor, where seven samples to be measured, Al2O3 (ε_r' = 9.34), Fe O23 (ε_r' = 4.5), FR4 (ε_r' = 4.4), Rogers RO4003 (ε_r' = 3.55), F4BM-2 (ε_r' = 3.5), PE (ε_r' = 2.26) and TEFLON (ε_r' = 2.1) were selected. Among them, Fe2O3 was in powder form. The samples to be tested were loaded on FR-4 dielectric plates of different sizes and their thicknesses were consistent as the thickness of the actual prepared material, and upon simulation of this, it was found that the conclusions were basically the same as long as the MUT covered the sensing cell. Therefore, the uniform physical size of the samples to be tested is 12.5mm*8.5mm, and the thicknesses of the seven samples to be tested are listed below, as shown in Table I.

Table I. Thickness of samples to be tested

MUT	Al O23	Fe O23	FR4	Rogers RO4003	F4BM-2	PE	TEFLON
Thickness (mm)	5	0.5	5	0.5	1	5	5

The simulated and measured results are shown in Fig. 10 and Fig. 11, respectively. In the figure, black solid line, red solid line, blue solid line, green solid line, purple solid line, ginger solid line, light blue solid line and brown solid line represent no load, loaded Al2O3, Fe2O3, FR4, Rogers RO4003, F4BM-2, PE and TEFLON respectively.

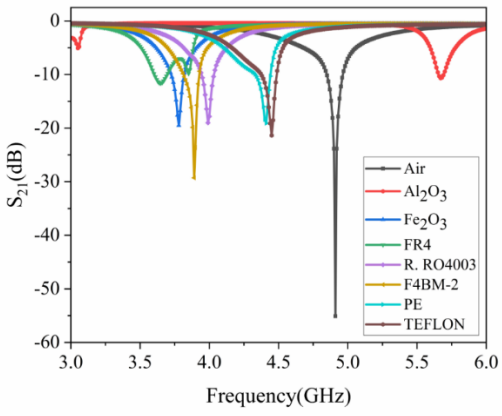

Fig. 10 Simulation results based on MCSRR sensor loaded with different MUTs

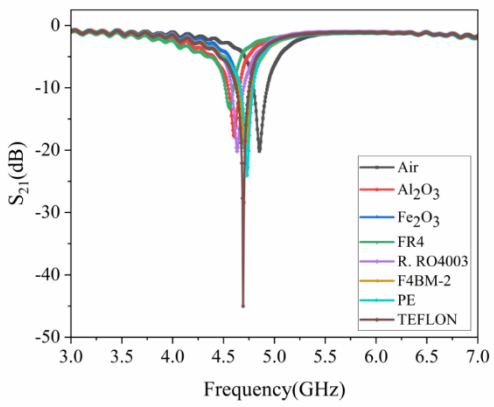

Fig. 11 Measured results based on MCSRR sensor loaded with different MUTs

As can be seen from the comparison of the data in Fig. 10 and Fig. 11, the simulation data and the measured data behave exactly the same when unloaded, while the S21 difference between the simulation data and the measured data is within 1 when the sample to be tested is loaded. The possible reasons for the error are as follows:

1) In the simulation process, the medium plate is set as a smooth plane model, and the sample to be measured shows a regular square structure; however, in the actual measurement, the smoothness of the medium plate cannot be ensured, and the shape of the sample to be measured may also have some irregularities;

2) Before the simulation of the sample to be measured, only the actual value of the dielectric constant was set and the loss tangent was set to 0. In actual measurements, the sample to be measured has a loss tangent in addition to the value of the dielectric constant;

3) In the actual measurement process, it is also necessary to consider the errors introduced by the SMA joints. The quality of the joints as well as the merit of the welding may interfere with the test results to a certain extent;

4) In the simulation process, the sample to be measured is tightly fitted to the dielectric plate, and there is no air gap in between. In actual measurement, however, the air gap between the sample to be measured and the dielectric plate is difficult to estimate accurately, and there is a difference in the data obtained whether the sample is placed directly or clamped. This small difference, even if it is only two decimal places, can lead to errors in the calculation of the dielectric constant;

5) In addition, the temperature and humidity of the indoor environment, as well as the warm-up and standby time of the vector network analyser, may also have some effect on the measurement data.

Finally, the dielectric constant was inverted by Eq. (8) and compared with the results in the literature as shown in Table II. In the table, the differences between the measured data and the literature data are expressed in percent.

Table II. Comparison of measured results of dielectric constant of MCSRR based sensors with literature data

MUT	Ref.	Measured Data	Different (%)
Al O23	9.34	9.44	1.07
Fe O23	4.5	4.14	8.70
FR4	4.4	5.33	21.14
Rogers RO4003	3.55	3.21	1.11
F4BM-2	3.5	3.63	3.71
PE	2.26	1.71	32.16
TEFLON	2.1	1.59	32.08

From the above table, it can be seen that FR4, PE and TEFLON three kinds of customised samples with a thickness of 5mm have larger measurement errors; while Fe2O3 , Rogers RO4003 and F4BM-2 three kinds of samples with a thickness of less than 5mm have better measurement results; in addition, since the main components of the temperature measurement ring used in the measurements are Al2O3 ceramics and their compounds, their dielectric constants are unclear; however, they have smaller errors than the other samples to be measured. However, compared with other samples to be measured, Al2O3 has the smallest error in the measurement results.

5. Conclusion

In this paper, an open-circuit microstrip line loaded Multiple Complementary Split-Ring Resonator (MCSRR) dielectric constant sensor is proposed. According to the theoretical calculation of the equivalent circuit and the analysis of electromagnetic field simulation, the equivalent element values are extracted, and the law of the resonance frequency change with the dielectric constant is obtained, which proves that the coupling capacitance between the resonators can enhance the sensitivity of the sensor. Finally, the physical sensor is processed and fabricated and measured, and the experimental results are in good agreement with the simulation results. This work verifies the feasibility of loading the MCSRR sensor.

References

[1] Gil M, Bonache J, Martin F. Synthesis and applications of new left handed micro-strip lines with complementary split-ring resonators etched on the signal strip [J]. IET Microwaves Antennas and Propagation, 2008, 2(4): 324-330.

[2] Kim Y J, Lee H M. Electrically small square loop antenna with a capacitive split ring resonator cover structure [J]. Microwave and Optical Technology Letters, 2009, 51(3): 831-835.

[3] Wang W, Gong S, Cui Z, et al. Dual band notched ultra-wideband antenna with co-directional SRR [J]. Microwave and Optical Technology Letters, 2009, 51(4): 1032-1034.

[4] Sunil J, Ashish D, Rajeev G, et al. A review: advancement in metamaterial based RF and microwave absorbers [J]. Sensors and Actuators: A. Physical, 2023, 354.

[5] Veselago V G, Narimanov E E. The left hand of brightness: past, present and future of negative index materials.[J]. Nature materials, 2006, 5(10): 759-62.

[6] Pendry, Holden, Stewart. Extremely low frequency plasmons in metallic mesostructures [J]. Physical Review Letters, 2001, 87(11):4773-4776.

[7] Smith D R, Schurig D, Pendry J B. Negative refraction of modulated electromagnetic waves [J]. Applied Physics Letters, 2002, 81(15): 2713-2715.

[8] Lu J, Grzegorczyk T, Zhang Y, et al. Cerenkov radiation in materials with negative permittivity and permeability [J]. Optics Express, 2003, 11(7): 723-34.

[9] Qing D K, Chen G. Goos-Hänchen shifts at the interfaces between left- and right-handed media [J]. Optics Letters, 2004, 29(8): 872.

[10] Schurig D, Mock J J, Justice B J, et al. Metamaterial electromagnetic cloak at microwave frequencies [J]. Science, 2006, 314: 977-980.

[11] Lee H-J, Yook J-G. Biosensing using split-ring resonators at microwave regime [J]. Applied Physics Letters, 2008, 92(25).

[12] Lee H-J, Lee H-S, Yoo K-H, et al. DNA sensing using split-ring resonator alone at microwave regime [J]. Journal of Applied Physics, 2010, 108(1).

[13] Dragoman M, Cismaru A, Radoi A, et al. DNA hybridization detection in a miniaturised electromagnetic band gap resonator [J]. Applied Physics Letters, 2011, 99(25).

[14] Pan W, Yan Y, Ma Y, et al. A terahertz metamaterial based on electromagnetically induced transparency effect and its sensing performance [J]. Optics Communications, 2019, 431(11): 5-9.

[15] Zhou H. Electromagnetic properties of artificial planar metamaterials and their sensing applications [D]. Chongqing University, 2020.

[16] Saha S, Bera S, Mandal H, et al. A temperature compensated non-contact pressure transducer using hall sensor and bourdon tube [J]. IEEE Sensors Journal, 2019, 19(14): 5429-5438.

[17] Horestani A K, Fumeaux C, Al-Sarawi S F, et al. Displacement Sensor Based on Diamond-Shaped Tapered Split Ring Resonator [J]. IEEE Sensors Journal, 2013, 13(4): 1153-60.

[18] Collette C, Fueyo R, Horodinca M, et al. Prototype of a small low noise absolute displacement sensor [J]. IEEE Sensors Journal, 2014, 14(1): 91-95.

[19] Horestani A K, Naqui J, Abbott D, et al. Two-dimensional displacement and alignment sensor based on reflection coefficients of open microstrip lines loaded with split ring resonators [J]. Electronics Letters, 2014, 50(8): 620-2.

[20] Horestani A K, Naqui J, Shaterian Z, et al. Two-dimensional alignment and displacement sensor based on movable broadside-coupled split ring resonators [J]. Sensors and Actuators A: Physical, 2014, 210: 18-24.

[21] Tian Ying. Research and design of metamaterial sensor based on open-slit ring resonator [D]. Central China Normal University, 2018.

[22] CHENG Fayong, ZHANG Kaihong, GUO Xiaoyu, et al. Research on temperature testing technology of digital temperature sensor[J]. Electronic Quality, 2021(10): 18-21.

[23] Lee C-S, Yang C-L. Complementary Split-Ring Resonators for Measuring Dielectric Constants and Loss Tangents [J]. IEEE Microwave and Wireless Components Letters, 2014, 24(8): 563-5.

[24] Galindo-Romera G, Herraiz-Martínez F J, Gil M, et al. Submersible Printed Split Ring Resonator-Based Sensor for Thin-Film Detection and Permittivity Characterisation [J]. IEEE Sensors Journal, 2016, 16(10): 3587-96.

[25] Hu Pepe. Theoretical and experimental study of CSRR characteristics [D]. North China Electric Power University, 2019.

[26] Albishi A M, Badawe M K E, Nayyeri V, et al. Enhancing the Sensitivity of Dielectric Sensors With Multiple Coupled Complementary Split-Ring Resonators [J]. IEEE Transactions on Microwave Theory and Techniques, 2020, 68(10): 4340-7.

[27] Zhang ZY. Research on the application of metamaterials in microwave dielectric constant sensors [D]. Jilin University, 2022.

[28] Singh S K, Tiwari N K, Yadav A K, et al. Design of ZnO/N-Doped Graphene Nanohybrid Incorporated RF Complementary Split Ring Resonator Sensor for Ammonia Gas Detection [J]. IEEE Sensors Journal, 2019, 19(18): 7968-75.

[29] Kiani S, Rezaei P, Navaei M. Dual-sensing and dual-frequency microwave SRR sensor for liquid samples permittivity detection [J]. MEASUREMENT, 2020, 160.

[30] Javadian-Saraf A, Hosseini E, Daniel Wiltshire B, et al. Graphene oxide/polyaniline-based microwave split-ring resonator: a versatile platform towards ammonia sensing [J]. Journal of Hazardous Materials, 2021, 418.

[31] Jian L, Xun C, Haoran W, et al. Temperature sensing technique by using a microwave photonics filter based on an actively mode-locked fiber laser [J]. Microwave and Optical Technology Letters, 2021, 63(10): 2535-2540.

[32] Sijie C, Pan P, Tongtong X, et al. Sensitivity enhanced fiber optic temperature sensor based on optical carrier microwave photonic interferometry with harmonic Vernier effect [J]. Optics and Laser Technology, 2023, 160.

[33] Dong Y, Zhang J, Zhang C, et al. Analysis and Design of Fiber Microprobe Displacement Sensors Including Collimated Type and Convergent Type for Ultra- Precision Displacement Measurement [J]. Micromachines, 2024, 15(2).

[34] Gan Hongyi. Design of high-performance and miniaturised planar microwave sensor based on complementary open resonant ring (CSRR)[D]. Hangzhou University of Electronic Science and Technology, 2021.

[35] Wang, D. X.. Research and design of dielectric constant test method based on resonant characteristics of microwave structures[D]. Chongqing University of Posts and Telecommunications, 2021.

[36] Li Yao. Research on pulse wave velocity measurement based on complementary open-ring resonator[D]. Dalian University of Technology, 2022.

[37] Hairong K, Libo Y, Xiaoyong Z, et al. Wireless Passive Microwave Antenna-Integrated Temperature Sensor Based on CSRR. [J]. Micromachines, 2022, 13(621): 1-10.

[38] Mohammed M, Bait S, et al. Detection of Reinforced Concrete Blocks Using Two-Port Microwave CSRR Sensor.[J]. IEEE Access, 2022, 10: 89437-89444.

[39] Zizhuo S, Huixin Z, Shaojun Z, et al. A Microwave CSRR Sensor for Non-Invasive Glucose-Level Detection.[J]. IEEE 5th International Conference on Electronic Information and Communication Technology (ICEICT), 2022, 872-874.

[40] Hong X, Sen Y, Cheng G, et al. A Dual-Scale CSRRs-Based Sensor for Dielectric Characterisation of Solid Materials. [J]. IEEE Sensors Council, 2022, 3502704.